Manuscript prepared for J. Name
with version 5.0 of the LaTeX class copernicus.cls.
Date: 5 February 2014

Analysis of the PKT correction for direct CO_2 flux measurements over the ocean

Sebastian Landwehr[1], Scott D. Miller[2], Murray J. Smith[3], Eric S. Saltzman[4], and Brian Ward[1]

[1]School of Physics and Ryan Institute, National University of Ireland Galway, Galway, Ireland
[2]Atmospheric Sciences Research Center, University at Albany, State University of New York, Albany, New York, USA
[3]National Institute of Water and Atmospheric Research (NIWA), Private Bag 14-901 Kilbirnie, Wellington, New Zealand
[4]Department of Earth Sciences, University of California, Irvine, CA, USA

Correspondence to: B. Ward (bward@nuigalway.ie)

Abstract. Eddy covariance measurements of air–sea CO_2 fluxes can be affected by cross-sensitivities of the CO_2 measurement to water vapour, resulting in order-of-magnitude biases. Well established causes for these biases are (i) cross-sensitivity of the broadband non-dispersive infrared sensors due to band-broadening and spectral overlap (commercial sensors typically correct for this) and (ii) the effect of air density fluctuations (removed by determining the dry air CO_2 mixing ratio). Another bias related to water vapour fluctuations has recently been observed with open-path sensors, attributed to sea salt build-up and water films on sensor optics. Two very different approaches have been used to deal with these water vapour-related biases. Miller et al. (2010) employed a membrane drier to physically eliminate 97 % of the water vapour fluctuations in the sample air before it entered a closed-path gas analyser. Prytherch et al. (2010a) employed the empirical (Peter K. Taylor, PKT) post-processing correction to correct open-path sensor data. In this paper, we test these methods side by side using data from the Surface Ocean Aerosol Production (SOAP) experiment in the Southern Ocean. The air–sea CO_2 flux was directly measured with four closed-path analysers, two of which were positioned down-stream of a membrane dryer. The CO_2 fluxes from the two dried gas analysers matched each other and were in general agreement with common parameterisations. The flux estimates from the un-dried sensors agreed with the dried sensors only during periods with low latent heat flux ($\leq 7\,\mathrm{W\,m^{-2}}$). When latent heat flux was higher, CO_2 flux estimates from the un-dried sensors exhibited large scatter and an order-of magnitude bias. Applying the PKT correction to the flux data from the un-dried analysers did not remove the bias when compared to the data from the dried gas analyser. The results of this study demonstrate the validity of measuring CO_2 fluxes using a pre-dried air stream and show that the PKT correction is not valid for the correction of CO_2 fluxes.

1 Introduction

Direct measurements of air–sea CO_2 flux contribute to the understanding of the Earth climate system and can be used to study the fundamental physics of air–sea gas exchange. When direct flux measurements are combined with the measurement of the partial pressure gradient of CO_2 across the air–water interface, ΔpCO_2, the gas transfer velocity k can be derived as follows (e.g. Wanninkhof, 1992):

$$k = \frac{F_\mathrm{c}}{S \cdot \Delta pCO_2} \tag{1}$$

where S is the solubility of CO_2 in sea water and F_c is the vertical CO_2 flux. The ability to parameterise k is essential for modelling global air–sea CO_2 fluxes based on ΔpCO_2 climatologies (Takahashi et al., 2002), and for increasing our understanding of the global oceanic uptake of CO_2 (Ward et al., 2004).

In the eddy covariance (EC) method, the turbulent flux is directly calculated from the covariance of the fluctuations in the vertical wind speed (w') and fluctuations in the CO_2 mixing ratio in dry air (x'_c):

$$F_\mathrm{c} = \langle n_\mathrm{d} \rangle \langle w' x'_\mathrm{c} \rangle \tag{2}$$

where n_d is the dry air density (here $\langle\ \rangle$ indicates a time average over a time interval t_I and the primes denote deviations from the mean). The w' and x'_c parameters need to be

sampled fast enough to resolve the smallest flux-carrying eddies (typically 10 Hz), and the averaging interval needs to be long enough to include large scale motions that contribute to the vertical flux, but short enough to ensure stationarity of the relevant parameters during the interval (typically t_I are between 15–60 min) (Kaimal et al., 1972). The EC method thus allows the study of gas transfer with much higher time resolution than both dual tracer experiments (e.g Nightingale et al., 2000; Ho et al., 2006) and measurements of the ^{14}C concentration in sea water (e.g Wanninkhof, 1992; Sweeney et al., 2007).

Commonly-used broadband infrared gas analysers (IRGA), such as LICOR LI7500 and LI7200, measure the CO_2 concentration n_c (number of molecules per volume), from which the mixing ratio needs to be calculated. Therefore, simultaneous measurements of temperature T, pressure P, and water vapour concentration n_v are necessary to calculate the dry air density $n_d = (P/RT - n_v)$ and the CO_2 mixing ratio $x_c = n_c n_d^{-1}$ (Webb et al., 1980). Equation (2) can be written as the sum of the flux measured by the IRGA and a bias flux, caused by the fluctuations of the dry air density, i.e.:

$$F_c = \underbrace{\langle n_c' w' \rangle}_{F_{IRGA}} + \underbrace{\langle x_c \rangle \cdot \left[\langle n_v' w' \rangle + \frac{\langle n_d + n_v \rangle}{\langle n_d \rangle} \cdot \left(\frac{\langle T' w' \rangle}{\langle T \rangle} - \frac{\langle P' w' \rangle}{\langle P \rangle} \right) \right]}_{F_q + F_T + F_P} \quad (3)$$

For CO_2, the bias terms (F_q, F_T and F_P) can easily exceed the vertical flux by an order of magnitude because the fluctuations x_c' are small compared to the background $\langle x_c \rangle$ (Webb et al., 1980). Equations (3) and (2) are fully equivalent.

EC is considered a standard method over land, but the application over the open ocean has proved to be more challenging. In the case of ship-based studies, the wind speed measurement needs to be carefully corrected for platform motion (e.g Edson et al., 1998; Miller et al., 2008). Over land, the pressure term in Eq. (3) can be ignored, but at sea the platform motion-induced pressure fluctuations can introduce a further bias flux as they may correlate with residuals of ship motion signal in the motion-corrected wind speed (Miller et al., 2010). CO_2 fluxes over the ocean are typically much smaller than over land, and with currently available sensor technology (e.g. Licor 7500/7200 have a resolution of 0.11 ppm at 10 Hz sample rate) , a relatively high air–sea gradients $\Delta pCO_2 \geq 40\,\mu atm$ is required to keep the uncertainty in the flux signal due to sensor resolution below 10 % (Rowe et al., 2011).

For EC, the trace gas measurement has to be carried out on the same air sample as the wind speed measurement. This can be done directly using an open-path (OP) IRGA, which is located close to the sonic anemometer (Kondo and Osamu, 2007; Yelland et al., 2009; Prytherch et al., 2010b). Alternatively, air can be pumped to a distant closed-path (CP) IRGA, at a sufficiently high flow rate (e.g. McGillis et al., 2001). This allows deliberate pre-conditioning of the air sample, such as removal of the temperature and water vapour fluctuations and the application of in-line particle filters to avoid the deposition of salt or dust particles on the sensor lenses. McGillis et al. (2001) were the first to carry out EC measurements of the air–sea CO_2 flux, which were in general agreement with common bulk flux formulae. Miller et al. (2010) developed a CP system where 97 % of the water vapour flux signal is removed by passing the air flow through a membrane dryer. This significantly lowered the magnitude of the air density correction term in Eq. (3).

Attenuation of the fluctuations within the sample tube of CP systems can lead to an underestimation of the turbulent transport carried by the small high frequency eddies (Leuning and King, 1992). To minimise this effect the flow must be kept fully turbulent (with a Reynolds number $Re \gtrsim 2100$). This requires flow rates ($\mathcal{O}(100)$ slpm). Therefore, CP systems have higher power and maintenance requirements than OP systems.

In the oceanic environment, the lenses of OP IRGAs are prone to the build-up of salt particles, and flushing with fresh water is necessary to avoid degradation of the signal. The LI7500 has also been deployed with a shroud and a very high airflow (570 slpm) (Edson et al., 2011). This deployment mode is a hybrid of the OP and CP mode as the contamination with sea spray is reduced with minimal loss of high frequency fluctuations. Even when the air density correction Eq. (3) has been applied carefully, reported CO_2 flux values based on OP and shrouded OP EC systems over the open ocean are typically an order of magnitude higher than expected based on generally accepted bulk flux parameterisations (Kondo and Osamu, 2007; Prytherch et al., 2010a; Lauvset et al., 2011; Edson et al., 2011).

The exact reason for the additional bias is still unclear. Kohsiek (2000) suggested that the build-up of water films on the sensor lenses could lead to a biased CO_2 measurement x_{cm} with dependency on the relative humidity (RH). This will cause a bias in the CO_2 flux measurement F_{cm}, which scales with the latent heat flux because the fluctuations of the water vapour concentration in the sample volume will lead to artificial fluctuations in x_{cm}. Removing this artificial cross-correlation is difficult because there is a natural correlation between the fluctuations of the two scalars x_c and x_v, which are both transported by the same turbulent eddies. Attempting to remove the artificial dependency $x_{cm}(RH)$ with regressions or polynomial fits can thus lead also to the removal of the turbulence-driven variations of x_c and, therefore, of the CO_2 flux signal itself. Prytherch et al. (2010a) suggested that the accumulation of salt particles on the lens of the LI7500 OP IRGA could modulate the magnitude of the bias. Edson et al. (2011) reported that the accumulation of salt particles on their shrouded and regularly cleaned IRGAs

was unlikely and suggested that a more suitable explanation was provided by the contamination of the optics with small particles from the ship's engines combined with organic deposits from sea spray. Prytherch et al. (2010a) went further and presented a correction method (called the Peter K. Taylor – PKT – method), which has since been used in several publications to correct OP CO_2 fluxes (e.g. Prytherch et al., 2010b; Lauvset et al., 2011; Edson et al., 2011; Huang et al., 2012; Ikawa et al., 2013). Huang et al. (2012) reported that the PKT correction did bring some of their CO_2 flux measurements closer to the bulk flux estimate, but found that for small water vapour fluxes the PKT method overcorrected the CO_2 flux and, in some cases, even resulted is a reversal of the flux direction. Ikawa et al. (2013) reported that the PKT correction resulted in incerased scatter when applied to coastal tower-based CO_2 flux measurements, and decided not to apply the correction. A selection of the publications mentioned above are also listed in Table 1 together with a brief description of the deployed IRGAs and findings relevant to this contribution.

Here we present direct CO_2 flux measurements performed during the Surface Ocean Aerosol Production (SOAP) experiment in the Southern Ocean, where we deployed the SUNY Albany Air/Sea Flux system (Miller et al., 2010), consisting of dried and un-dried CP IRGAs. In order to rule out that the failure of an individual IRGA would suggest differences between the dried and un-dried deployment, the number of IRGAs was doubled using sensors from NUIG.

We show that even EC measurements using CP IRGAs can be affected by a large humidity bias when the sampled air is neither dried nor filtered. We applied the PKT method (which does not include any OP-specific assumptions) to the un-dried CP data as a test of its ability to remove the observed humidity flux-related bias in broadband non-dispersive infrared (NDIR) sensors. We further analyse and discuss this correction method (Prytherch et al., 2010a) in detail.

2 Experiment and methods

The SOAP field campaign was conducted from February to March 2012 on the R/V *Tangaroa*. The EC system described here consisted of two Csat3 sonic anemometers attached to the bow mast (12.6 m a.s.l.), which provide high frequency measurements of the three components of the wind vector (u, v and w) and the speed of sound temperature (T_s), as well as four IRGAs of the type LI7200 ($\times 2$) and LI7500 ($\times 2$), which were located inside the container laboratory on the bow deck and connected to the sample volume on the mast with a stainless steel tube (ID = 1 cm; $L = 20$ m). The inlet tube was heated to avoid condensation on the walls, which would lead to an underestimation of the EC latent heat flux. Although the tubing had an inbuilt self-regulated heating resistor (Parker SL-522-B0849A), the temperature in the tubing was not measured continuously. However the LICOR temperature sensors recorded temperatures ranging from 23°C to 36°C at an outside air temperature ranging from 8°C to 16°C. A pump (Gast model 1423) delivered a continuous air stream from the mast at 100 slpm ($Re \approx 7500$), where Re is compute as $Re = \frac{Q \cdot 2R}{\nu \cdot \pi R^2}$, with the flow rate $Q\,[\mathrm{ms}^{-1}]$, the inner radius of the tubing $R\,[\mathrm{m}]$ and the kinematic viscosity of air $\nu \approx 7.1 \cdot 10^{-6} \mathrm{m}^2\mathrm{s}^{-1}$. Figure 1 shows a schematic of the flux system.

A part of the main flow (17 slpm; ID = 6 mm; $L = 2$ m; $Re \approx 2100$) was directed to the two LI7200s CP IRGAs (*wetA*, *wetB*) connected in sequence. Up to this point the air was not filtered. The air stream was subsequently divided and passed to two LI7500s, which were connected in parallel. The 7500 OP units were converted to CP and each one was positioned downstream of a Nafion membrane dryer (PD-200T) to remove fast water vapour fluctuations as shown by Miller et al. (2010). They are described as (*dryA* and *dryB*) in the following text.

Zero air was injected periodically (every 6 h) into the sample inlet to measure the delay of the signal in the IRGAs. Pressure and temperature in each IRGA sample volume were also measured with external sensors (Mensor CPT6100 and a thermocouple, respectively). An inertial motion unit (IMU – Systron Donner MotionPak II) provided high frequency acceleration and rate data, and a GPS compass and the ship's gyrocompass were used to completely describe the ship's motion. These data allowed the wind speed measurements from the Csat3 to be corrected for platform motion following Miller et al. (2008). All measurements were performed at 10 Hz.

2.1 Data analysis and flux calculations

The fluxes of momentum u_* and the sonic sensible heat H_{sonic} were calculated from the Csat3 data after motion correction (Miller et al., 2008) and rotation of the wind vector into the mean flow (McMillen, 1988). The latent heat flux Hl was calculated from the covariance of the vertical wind speed w with the water vapour mixing ratio x_v from *wetA* and *wetB* after correction for the time delay. H_{sonic} was corrected with the latent heat flux to derive the sensible heat flux H_s, following (Burns et al., 2012). The measured CO_2 density was converted into mixing ratio (as described in Sect. 1) and ship motion contaminations of the signal due to flexing of the sensor or inertial forces on the filter wheel were removed using a linear regression with the acceleration and rate signal (as in Miller et al., 2010).

All flux calculations were performed over 25 min intervals. These intervals were divided into five 5 min subintervals and were excluded if any of the mean wind direction within the sub-intervals exceeded $\pm 100°$ to the bow to minimise flow distortion effects. Flux intervals were also excluded when spikes were present in the wind speed or IRGA measurements. The remaining intervals were checked for signs of non-stationarity in the CO_2 co-spectra of the

dryA and *dryB*, and the same criteria as in Bell et al. (2013) were applied. It has to be noted here, that the co-spectra of CO_2 and H_2O are similar. Therefore a cross-contamination of the CO_2 signal with H_2O cannot be clearly identified by spectral analysis. A total of 327 from the 1039 available intervals passed the quality control for *dryA* as well as for *dryB* and were used for the analysis presented here. For *wetA* and *wetB*, only 273 and 269 intervals, respectively, passed because these analysers had been removed from the setup for about one day. Flux measurements from *wetA* and *wetB* passed both for 267 intervals, because spikes had compromised the data from the two sensors during different intervals.

The PKT correction, as presented by Prytherch et al. (2010a), was applied to the mixing ratios measured by the two analysers *wetA* and *wetB*. This method includes an iteration in which the correct flux value is approximated. The termination criteria for the iteration was chosen according to Prytherch et al. (2010a), to be $|F_c^{(j)} - F_c^{(j-1)}| \leq 0.04\,\mathrm{mol\,m^{-2}\,yr^{-1}}$. Prytherch et al. (2010a) also suggested a rejection of the PKT results if the iteration did not converge within 10 steps or if $F_c^{(j)}$ exceeded $\pm 400\,\mathrm{mol\,m^{-2}\,yr^{-1}}$ (which was considered unrealistically high). Thus the application of the PKT correction to the measurements from the un-dried IRGA lead to a further reduction of the data set. For *wetA*, the PKT correction rejected 102 of the 273 intervals and for *wetB* 89 of 269, respectively. Flux measurements and PKT results passed for both sensors for 161 of the intervals. The fluxes calculated from measured x_{cm} and the PKT-corrected x_{PKT} were evaluated against the unbiased measurements of the dried IRGAs. These results are presented in Sects. 3.1 and 3.2, respectively.

The flux measurements are affected by air-flow distortion, which results in a bias that depends mostly on the relative wind direction (Popinet et al., 2004; O'Sullivan et al., 2013). For this submission, the flux measurements were not corrected for air flow distortion because we concentrate on the comparison of different IRGA signals that were all correlated with the same wind speed measurement. Air flow distortion does therefore not affect our conclusions.

3 Results

Figure 2 shows an overview of the conditions encountered during the SOAP experiment from 16 February to 5 March 2012 (doy 47–65). The wind speed range was between 0–15 $\mathrm{m\,s^{-1}}$ (25 min average) and peaked at $20\,\mathrm{m\,s^{-1}}$ on doy 61. Unfortunately, the uninterruptible power supply of the EC system was flooded during this storm event, leading to a 12 h gap in the record. The ship was steered into the wind as much as possible, except during survey periods or deployments of instruments. The air temperature was mostly colder than the water temperature (measured by the ship's thermosalinograph) except for a period between doy 51 and 55, when a warm air mass led to negative turbulent heat fluxes. The air-water pCO_2 difference ranged between $-40\,\mu\mathrm{atm}$ and $-120\,\mu\mathrm{atm}$. These large ΔpCO_2 values were easily within the $40\,\mu\mathrm{atm}$ criterion for EC flux measurements with the LICOR IRGAs (Rowe et al., 2011).

3.1 Primary CO_2 flux results

The CO_2 flux measurements from the four CP IRGAs (without PKT correction) are plotted in Fig. 3 (top and middle). The CO_2 flux estimates from the dry gas analysers were in general agreement with each other and Sweeney et al. (2007), which is an updated version of the widely-used parameterisation from Wanninkhof (1992), while the flux measurements from the un-dried gas analysers exhibited large scatter.

The LICOR IRGAs measure CO_2 density and the measured flux signal F_{IRGA} must be corrected for the air-density flux bias terms (F_q, F_T, and F_P) to obtain the correct CO_2 flux signal F_c. The flux bias terms at different measurement positions are shown in Fig. 4. For the un-dried IRGA F_q exceeded F_c by an order of magnitude (Fig. 4 top). For the whole data set, the average magnitude of the latent heat flux from the un-dried IRGAs was $36\,\mathrm{W\,m^{-2}}$, in contrast the average magnitude of the latent heat flux downstream of the dryer was $2.4\,\mathrm{W\,m^{-2}}$. The application of the diffusion dryer therefore reduced F_q in average by 93 %. This is comparable to (Miller et al., 2010), who found a reduction by 97 %. A similar effective reduction was found for F_T (Fig. 4 bottom), when compared with the open-path measurement by the sonic anemometer. The reduction of F_T is due to heat exchange of the sample air with the 20 m long inlet tubing and does not depend upon the drying. F_P (Fig. 4 bottom) is much smaller than F_q and F_T, but of the same magnitude as F_c. F_P cannot be reduced physically and needs to be measured accurately (Miller et al., 2010).

The flux measurement of all four CP-IRGAs, as presented in Fig. 3, have been corrected for the air-density bias fluxes by calculating the CO_2 mixing ratio. However, even after this correction was applied, the un-dried IRGA CO_2 fluxes showed erratic behaviour. The difference in the CO_2 flux measurements from the un-dried and dried IRGAs is plotted in Fig. 5. The variance of the flux data from *wetA* and *wetB* increased proportionally with the latent heat flux and became an order of magnitude larger than that from *dryA* or *dryB*. There was no apparent correlation between the differences in the CO_2 fluxes ΔF and the bias fluxes caused by the pressure and temperature fluctuations (F_T, and F_P).

It has to be pointed out that the primary flux measurements from the two un-dried sensors agreed with the measurements from the dried IRGAs during periods with very low latent heat flux ($Hl \leq 7\,\mathrm{W\,m^{-2}}$). These periods are marked as shaded areas in Figs. 2 and 3. The limit of $7\,\mathrm{W\,m^{-2}}$ was chosen so that the envelope of the bias was approximately two times the scatter observed at $Hl \approx 0\,\mathrm{W\,m^{-2}}$. Figure 6 shows scatter plots of the flux measurements from *wetA* and

wetB against those from *dryB* for ($\mathrm{Hl} \leq 7\,\mathrm{W\,m^{-2}}$) and of *dryA* against *dryB* for the whole data set. A linear regression of the *dryA* vs. *dryB* for the full dataset gave a slope of (1.09 ± 0.01) with a $R^2 = 0.96$. For *wetA* and *wetB* regression was performed over the restricted data set ($\mathrm{Hl} \leq 7\,\mathrm{W\,m^{-2}}$) and gave slopes of (0.88 ± 0.15) with $R^2 = 0.36$ and (0.93 ± 0.06) with $R^2 = 0.78$, respectively.

Figures 7 and 8 (left side) show scatter plots of the primary flux measurements of *wetA* and *wetB* against *dryB* for the full data set. The magnitude of the latent heat flux is used as colour code. Linear regression gave a slope of (-0.17 ± 0.8) for *wetA* vs. *dryB* and $(+0.7 \pm 0.2)$ for *wetB* vs. *dryB*, respectively, both with very low R^2 values. On average, the effect of the bias was to reduce the CO_2 flux, even changing the sign.

3.2 Application of the PKT Correction to the flux measurements from the un-dried IRGAs

The PKT correction, as presented by (Prytherch et al., 2010a), was applied to the x_{cm} measured by the two un-dried analysers and the results were evaluated against the unbiased measurements of the dried IRGAs. Figure 3 (bottom) shows the PKT-corrected fluxes ($F_{\mathrm{c}}^{\mathrm{PKT}}$) as well as the results from Eq. (7), which is derived in Sect. 4 and presents a simplified version of the PKT correction that also provides an output when the PKT correction does not converge. The results of Eq. (7) are not used in the evaluation of the PKT correction results, i.e. intervals that were rejected by the PKT correction are excluded from the analysis.

Scatter plots in Figs. 7 and 8 show the correlation between the flux measurements form the un-dried IRGAs and the fluxes from *dryB* before (left) and after the application of the PKT correction to the un-dried measurements (right). For low latent heat flux, the PKT correction increases the scatter of the initially well-correlated measurements and also rejects a large part of the results. For *wetA*, the PKT correction reduces the large range of scatter, but does not improve the correlation with the *dryB* fluxes. For *wetB*, which shows a weaker bias, the PKT correction even reduces the correlation with the *dryB* flux estimates from (0.7 ± 0.2) to (0.4 ± 0.2).

The average raw flux estimates from the four CP IRGAs and with PKT correction for the two un-dried IRGAs are shown in Table 2. The average was taken over the 161 intervals, where PKT results were available for both un-dried gas analyser, and over three subsets, which were based on the magnitude and sign of the latent heat flux measured by the un-dried IRGAs. For the whole cruise, the PKT correction brought the flux measurements from *wetA* and *wetB* into closer agreement. The mean estimate of *wetA* and *wetB* after PKT did, however, underestimate the flux ($\overline{F_{\mathrm{c}}} = -7.19\,\mathrm{mol\,m^{-2}\,yr^{-1}}$) by 62 % . For Subset 1, ($[-7\,\mathrm{W\,m^{-2}} \leq \mathrm{Hl} \leq +7\,\mathrm{W\,m^{-2}}]$) the bias in the un-dried IRGA was negligible and the flux estimates of all four sensors agreed within 10 %. Here PKT correction changed the results by less than 12 %. For Subset 2 with moderately negative latent heat fluxes ($[-35\,\mathrm{W\,m^{-2}} \leq \mathrm{Hl} \leq -7\,\mathrm{W\,m^{-2}}]$), the PKT correction increased the bias in the flux measurements from 25 % to 48 %. Subset 3 included the largest latent heat fluxes ($[+7\,\mathrm{W\,m^{-2}} \leq \mathrm{Hl} \leq 340\,\mathrm{W\,m^{-2}}]$); here, the PKT-corrected fluxes are only small fractions of the dried fluxes i.e. $\leq 1\,\%$ and 14 % for *wetA* and *wetB*, respectively. The average flux estimates of the two dried IRGAs agreed within 1 % for the whole cruise and for each of the subsets 1 and 3. For subset 2 the agreement was within 3 %.

4 Analysis of the PKT correction

To investigate the unsatisfactory results of the PKT correction (cp. Sect. 3.2), we will now analyse the correction algorithm in detail.

The PKT method Prytherch et al. (2010a) is based on the assumption that the ratio of the variations of two quantities, e.g., CO_2 and relative humidity, is equal to the ratio of their vertical fluxes:

$$\frac{\partial \langle x_{\mathrm{c}} \rangle}{\partial \langle \mathrm{RH} \rangle} = \frac{\langle x_{\mathrm{c}}' w' \rangle}{\langle \mathrm{RH}' w' \rangle} \tag{4}$$

Prytherch et al. (2010a) derived Eq. (4) from the Monin–Obhukov similarity theory, assuming that the scalar profiles of the two non-dimensionalised quantities are equal.

The correction algorithm can be summarised as follows: first, the variations of x_{c} that are dependent on RH are removed from the measured signal x_{cm} with a 3rd order polynomial fit to the x_{cm} and RH time series:

$$x_{\mathrm{c}}^{(0)} = x_{\mathrm{cm}} - \sum_{n=1:3} a_n (\mathrm{RH})^n \tag{5}$$

where a_j are the polynomial coefficients determined by the fit. A first-step CO_2 flux $F_{\mathrm{c}}^{(0)}$ is calculated from the detrended signal $x_{\mathrm{c}}^{(0)}$, and then used with Eq. (4) to get a first approximation of $\frac{\partial \langle x_{\mathrm{c}} \rangle}{\partial \langle \mathrm{RH} \rangle}$. The CO_2 mixing ratio is then adjusted using this quantity:

$$x_{\mathrm{c}}^{(\mathrm{new})} = x_{\mathrm{c}}^{(0)} + 0.5 \cdot (\mathrm{RH}') \cdot \frac{F_{\mathrm{c}}^{(0)}}{\langle x_{\mathrm{v}}' w' \rangle} \frac{\partial \langle x_{\mathrm{v}} \rangle}{\partial \langle \mathrm{RH} \rangle} \tag{6}$$

Here, the relative humidity flux $\langle \mathrm{RH}' w' \rangle$ was substituted with $\langle x_{\mathrm{v}}' w' \rangle (\frac{\partial \langle x_{\mathrm{v}} \rangle}{\partial \langle \mathrm{RH} \rangle})^{-1}$, similar to Eq. (4). The adjusted time series $x_{\mathrm{c}}^{(\mathrm{new})}$ is now used to calculate an approximation of the CO_2 flux, and produce a new correction term via via Eq. (4) to be used in Eq. (6). Equations (4) and (6) are then looped until the CO_2 flux estimate converges to a flux value $F_{\mathrm{c}}^{\mathrm{PKT}}$ (this loop typically converges within less than 10 steps). Equations (4–6) are taken from the Matlab code in the supplementary material of Prytherch et al. (2010a).

We found that the loop can be replaced by one simple equation:

$$F_{\mathrm{c}}^{\mathrm{PKT}} = F_{\mathrm{c}}^{(0)} \cdot \beta \tag{7}$$

where $\beta = \left(1 - 0.5 \frac{\langle \mathrm{RH}' w' \rangle}{\langle x_{\mathrm{v}}' w' \rangle} \frac{\partial \langle x_{\mathrm{v}} \rangle}{\partial \langle \mathrm{RH} \rangle}\right)^{-1}$. From Eq. (4) it follows that $\beta \approx 2$.

In order to show this, we re-write Eq. (6) by replacing the adjusted mixing ratio $x_{\mathrm{c}}^{(\mathrm{new})}$ with $x_{\mathrm{c}}^{(j)}$ and $F_{\mathrm{c}}^{(0)}$ with the flux from the previous iteration step $F_{\mathrm{c}}^{(j-1)}$:

$$x_{\mathrm{c}}^{(j)} = x_{\mathrm{c}}^{(0)} + 0.5 \cdot (\mathrm{RH}') \cdot \frac{F_{\mathrm{c}}^{(j-1)}}{\langle x_{\mathrm{v}}' w' \rangle} \frac{\partial \langle x_{\mathrm{v}} \rangle}{\partial \langle \mathrm{RH} \rangle} \tag{8}$$

Equation (8) is iterated within the PKT loop. The new flux estimate of iteration j (i.e. $F_{\mathrm{c}}^{(j)}$) is computed from $x_{\mathrm{c}}^{(j)}$ as follows:

$$F_{\mathrm{c}}^{(j)} = F_{\mathrm{c}}^{(0)} + 0.5 \cdot \langle \mathrm{RH}' w' \rangle \cdot \frac{F_{\mathrm{c}}^{(j-1)}}{\langle x_{\mathrm{v}}' w' \rangle} \frac{\partial \langle x_{\mathrm{v}} \rangle}{\partial \langle \mathrm{RH} \rangle} \tag{9}$$

and is used to compute $x_{\mathrm{c}}^{(j+1)}$ via Eq. (8). However, if Eq. (9) is inserted into the convergence criterion ($F_{\mathrm{c}}^{(j)} - F_{\mathrm{c}}^{(j-1)} \rightarrow 0$) and solved for $F_{\mathrm{c}}^{(j-1)}$, we find that the loop will terminate at $F_{\mathrm{c}}^{\mathrm{PKT}}$ given by Eq. (7). The results of the loop agree with Eq. (7) within the tolerance $|F_{\mathrm{c}}^{(j)} - F_{\mathrm{c}}^{(j-1)}| \leq 0.04\,\mathrm{mol\,m^{-2}\,yr^{-1}}$, which is used by Prytherch et al. (2010a) to determine that the loop has converged. In Fig. 9 the results from Eq. (7) and the PKT loop are plotted over the 1:1 correspondence line. A significant advantage of Eq. (7) is that it always provides a result whereas the PKT loop does not always converge. In Fig. 3 (bottom) the results of Eq. (7) are overlaid with $F_{\mathrm{c}}^{\mathrm{PKT}}$. The rejection criteria in the PKT correction algorithm lead to a reduced range of scatter in the PKT results when compared to the results of Eq. (7).

Prytherch et al. (2010a) validated the PKT method by applying it to the sensible heat flux (F_{Ts}) as calculated from the measured speed of sound temperature (T_{s}). We followed this analysis and show our results in Fig. 10, which can be directly compared to Fig. 2 in (Prytherch et al., 2010a). The average of the flux, calculated from the detrended sonic temperature ($F_{\mathrm{Ts}}^{(0)}$), yields approximately one half of the flux signal. The PKT flux, which is equal to the product of the detrended flux and β, correlates with the standard EC sensible heat flux. The factor 0.5 in Eq. (7) comes from the same factor Eq. (6), which was originally inserted to reduce the step width and improve the convergence of the iteration and was not expected to change the result of the PKT correction (J. Prytherch, review comments). In order to illustrate the influence of this factor, the results of a PKT correction with a factor of 0.75 are shown in Fig. 10. Here $\beta \approx 4$ and the PKT results are ($\approx 4 \times F_{\mathrm{Ts}}^{(0)}$) and ($\approx 2 \times Hs$).

5 Discussion

The good agreement between the dried and un-dried CP systems for low latent heat fluxes (cp. Sect. 3.1) supports the findings of Miller et al. (2010) that application of a diffusion dryer does not alter the CO_2 flux signal, but avoids contamination of the sensor optics and significantly reduces the magnitude of the necessary air density correction.

The magnitude and scatter of the bias in the CO_2 flux results from the un-dried CP systems increased with the latent heat flux. These results are similar to results reported for OP IRGAs (LICOR-7500) (e.g Kondo and Osamu, 2007; Lauvset et al., 2011; Prytherch et al., 2010b), which showed an overestimation of the CO_2 flux magnitude, when compared to common bulk formulae. In this study, on the other hand, the bias reduced the CO_2 flux on average. Kondo and Tsukamoto (2012) simultaneously deployed OP (LICOR-7500) and CP (LICOR-7000) sensors to measure CO_2 fluxes in conditions with low air–sea CO_2 gradient ($12\,\mu\mathrm{atm} < \Delta pCO_2 < 42\,\mu\mathrm{atm}$) and large latent heat fluxes ($70\,\mathrm{W\,m^{-2}} \leq \mathrm{Hl} \leq 140\,\mathrm{W\,m^{-2}}$). The EC CO_2 flux estimates from both OP and CP IRGAs were an order of magnitude higher than expected using the Sweeney et al. (2007) parameterisation and diverged increasingly for higher latent heat fluxes. We therefore assume that the bias observed in the fluxes from the un-dried CP has the same origin as the biases observed in the OP measurements cited above. Our measurements also indicate that the bias can be different for each individual IRGA unit.

Equation (7) explains why the PKT correction produces unsatisfactory flux results: the PKT-corrected flux is simply a product of the flux signal, which was calculated from the CO_2 mixing ratios after detrending against the relative humidity, and the term $\beta \approx 2$ that depends solely on water vapour and relative humidity fluctuations. The ratio of the detrended fluxes of the two un-dried IRGAs to the CO_2 flux measured by the *dryB* and the factor β are plotted in Fig. 11 as a function of the latent heat flux. The parameter β shows a large scatter for low Hl but converges to 2 for $\mathrm{Hl} > 50$ $\mathrm{Wm^{-2}}$. The ratio of the detrended fluxes to the fluxes measured by the sensor *dryB* ($(F_{\mathrm{c}}^{0}) \cdot (F_{\mathrm{c}})^{-1}$) is on average close to 1 when latent heat flux is small, but exhibits large scatter. For $\mathrm{Hl} > 50$ $\mathrm{Wm^{-2}}$ the value of F_{c}^{0} becomes much smaller than F_{c}; this leads to the observed underestimation by the PKT-corrected fluxes.

The PKT correction appears to correct the latent heat flux bias in the sonic sensible heat flux, because the flux calculated from the detrended sonic temperature yields on average approximately one half of the flux signal and is then multiplied with $\beta \approx 2$. However, this does not prove that the PKT correction can successfully remove the bias in the measured CO_2 fluxes.

6 Conclusions

Measurements of the air–sea CO_2 flux over the open ocean were conducted with four IRGAs, two of which had the water vapour fluctuations removed with a membrane dryer (Miller et al., 2010). The flux results from the dried and un-dried sensors agreed with each other during periods of very low latent heat flux, demonstrating that the membrane dryer does not alter the CO_2 flux signal. With increasing latent heat flux, the CO_2 flux measurements from the un-dried sensors showed large bias and scatter. This is similar to earlier studies Kondo and Osamu (2007); Lauvset et al. (2011); Prytherch et al. (2010a). In this study the bias flux was positive (on average) leading to a net reduction of the downward CO_2 flux.

The PKT correction reduced the scatter in the flux measurements from the un-dried gas analysers from 1000 % to 100 % of the flux signal. However, the PKT-corrected fluxes showed only a weak correlation with the flux measurements from the dried gas analysers. A detailed analysis of the PKT algorithm was performed, which revealed that the loop in the PKT correction can be replaced by a single equation. The PKT-corrected flux was shown to be a product of the detrended CO_2 flux and a factor that depends solely on the latent heat flux and relative humidity. The PKT method cannot be used to retrieve the true CO_2 from the measured signal, since detrending to remove the bias also removes most of the CO_2 flux information. Conclusions made based on PKT-corrected CO_2 flux measurements should be treated with care.

The results support the conclusions of Miller et al. (2010) that the order of magnitude bias in the measured CO_2 fluxes can be removed when the sample air is dried. The authors therefore strongly recommend the use of the closed-path IRGAs with a diffusion dryer as presented by Miller et al. (2010) for EC flux measurements over the open ocean.

Acknowledgements. This research was funded by Science Foundation Ireland as part of the US-Ireland R&D Partnership Programme under Grant Number 08/US/I1455 and US National Science Foundation Award 0851407, and by NIWA under Atmosphere Research Programme 2. Additional funding was provided by a SFI Short-term Travel Fellowship under Grant 09/US/I1758-STTF-11, and the EU FP7 project CARBOCHANGE under grant agreement no. 264879. We thank the captain and crew of the R/V *Tangaroa* who supported the measurements. We thank Kim Currie for providing the ΔpCO_2 data. Also we want to express our gratitude to the reviewers John Prytherch, Margaret J. Yelland and Mingxi Yang.

References

Bell, T. G., De Bruyn, W., Miller, S. D., Ward, B., Christensen, K., and Saltzman, E. S.: Air-sea dimethylsulfide (DMS) gas transfer in the North Atlantic: evidence for limited interfacial gas exchange at high wind speed, Atmos. Chem. Phys., 13, 11073–11087, doi:doi:10.5194/acp-13-11073-2013, 2013.

Burns, S. P., Horst, T. W., Jacobsen, L., Blanken, P. D., and Monson, R. K.: Using sonic anemometer temperature to measure sensible heat flux in strong winds, Atmos. Meas. Tech., 5, 2095–2111, doi:10.5194/amt-5-2095-2012, 2012.

Edson, J. B., Hinton, A. A., Prada, K. E., Hare, J. E., and Fairall, C. W.: Direct covariance flux estimates from mobile platforms at sea, J. Atmos. Ocean. Tech., 15, 547–562, 1998.

Edson, J. B., Fairall, C. W., Bariteau, L., Zappa, C. J., Cifuentes-Lorenzen, A., McGillis, W. R., Pezoa, S., Hare, J. E., and Helmig, D.: Direct covariance measurement of CO_2 gas transfer velocity during the 2008 Southern Ocean Gas Exchange Experiment: wind speed dependency, J. Geophys. Res.-Oceans, 116, C00F10, doi:10.1029/2011JC007022, 2011.

Ho, D., Law, C., Smith, M., Schlosser, P., Harvey, M., and Hill, P.: Measurements of air–sea gas exchange at high wind speeds in the Southern Ocean: implications for global parameterizations, Geophys. Res. Lett., 33, L16611, doi:10.1029/2006GL026817, 2006.

Huang, Y., Song, J.,Wang, J., and Fan, C.: Air-sea carbon-dioxide flux estimated by eddy covariance method from a buoy observation, Acta Oceanol. Sin., 31, 66–71,doi:10.1007/s13131-012-0253-5, 2012.

Ikawa, H., Faloona, I.,Kochendorfer, J., Paw U, K., T., and Oechel, w., C.: Air–sea exchange of CO_2 at a Northern California coastal site along the California Current upwelling system, Biogeosciences, 10, 4419—4432,doi:www.biogeosciences.net/10/4419/2013/, 2013.

Kaimal, J. C., Wyngaard, J. C., Izumi, Y., and Coté, O. R.: Spectral characteristics of surface-layer turbulence, Q. J. Roy. Meteor. Soc., 98, 563–589, 1972.

Kohsiek, W.: Water vapor cross-sensitivity of open path H_2O/CO_2 sensors, J. Atmos. Ocean. Tech., 17, 299–311, 2000.

Kondo, F. and Osamu, T.: Air–sea CO_2 flux by eddy covariance technique in the equatorial indian ocean, J. Oceanogr., 63, 449–456, 2007.

Kondo, F. and Tsukamoto, O.: Comparative CO_2 flux measurements by eddy covariance technique using open- and closed-path gas analysers over the Equatorial Pacific Ocean, Tellus B, 64, 17511, doi:10.3402/tellusb.v64i0.17511, 2012.

Lauvset, S. K., McGillis, W. R., Bariteau, L., Fairall, C. W., Johannessen, T., Olsen, A., and Zappa, C. J.: Direct measurements of CO_2 flux in the Greenland Sea, Geophys. Res. Lett., 38, L12603, doi:10.1029/2011GL047722, 2011.

Leuning, R. and King, K. M.: Comparison of eddy-covariance measurements of CO_2 fluxes by open- and closed-path CO_2 analysers, Bound.-Lay. Meteorol., 59, 297–311, 1992.

McGillis, W., Edson, J., Hare, J., and Fairall, C. W.: Direct covariance air–sea CO_2 fluxes, J. Geophys. Res., 106, 16729–16745, 2001.

McMillen, R.: An eddy correlation technique with extended applicability to non-simple terrain, Bound.-Lay. Meteorol., 43, 231–245, doi:10.1007/BF00128405, 1988.

Miller, S., Hristov, T., Edson, J., and Friehe, C.: Platform motion effects on measurements of turbulence and air–sea exchange over the open ocean, J. Atmos. Ocean. Tech., 25, 1683–1694, 2008.

Miller, S. D., Marandino, C., and Saltzman, E. S.: Ship-based measurement of air–sea CO_2 exchange by eddy covariance, J. Geophys. Res., 115, D02304, doi:10.1029/2009JD012193, 2010.

Nightingale, P. D., Malin, G., Law, C. S., Watson, A. J., Liss, P. S., Liddicoat, M. I., Boutin, J., and Upstill-Goddard, R. C.: In situ evaluation of air–sea gas exchange parameterizations using novel conservative and volatile tracers, Global Biogeochem. Cy., 14, 373–387, 2000.

O'Sullivan, N., Landwehr, S., and Ward, B.: Mapping flow distortion on oceanographic platforms using computational fluid dynamics, Ocean Sci., 9, 855–866, doi:10.5194/os-9-855-2013, 2013.

Popinet, S., Smith, M., and Stevens, C.: Experimental and numerical study of the turbulence characteristics of airflow around a research vessel, J. Atmos. Ocean. Tech., 21, 1575–1589, 2004.

Prytherch, J., Yelland, M. J., Pascal, R. W., Moat, B. I., Skjelvan, I., and Neill, C. C.: Direct measurements of the CO_2 flux over the ocean: development of a novel method, Geophys. Res. Lett., 37, L03607, doi:10.1029/2009GL041482, 2010a.

Prytherch, J., Yelland, M. J., Pascal, R. W., Moat, B. I., Skjelvan, I., and Srokosz, M. A.: Open ocean gas transfer velocity derived from long-term direct measurements of the CO_2 flux, Geophys. Res. Lett., 37, L23607, doi:10.1029/2010GL045597, 2010b.

Rowe, M. D., Fairall, C. W., and Perlinger, J. A.: Chemical sensor resolution requirements for near-surface measurements of turbulent fluxes, Atmos. Chem. Phys., 11, 5263–5275, doi:10.5194/acp-11-5263-2011, 2011.

Sweeney, C., Gloor, E., Jacobson, A. R., Key, R, M., McKinley, G., Sarmiento, J. L., and Wanninkhof, R.: Constraining global air-sea gas exchange for CO_2 with recent bomb $^{1}4C$ measurements, Global Biogeochemical Cycles,21,1944-9224, doi:10.1029/2006GB002784,2007.

Takahashi, T., Sutherland, S. C., Sweeney, C., Poisson, A., Metzl, N., Tilbrook, B., Bates, N., Wanninkhof, R., Feely, R. A., Sabine, C., Olafsson, J., and Nojiri, Y.: Global sea–air CO_2 flux based on climatological surface ocean pCO_2, and seasonal biological and temperature effects, Deep-Sea Res. Pt. II, 49, 1601–1622, doi:10.1016/S0967-0645(02)00003-6, 2002.

Wanninkhof, R.: Relationship between wind speed and gas exchange, J. Geophys. Res., 97, 7373–7382, 1992.

Ward, B., Wanninkhof, R., McGillis, W. R., Jessup, A. T., DeGrandpre, M. D., Hare, J. E., and Edson, J. B.: Biases in the air–sea flux of CO_2 resulting from ocean surface temperature gradients, J. Geophys. Res., 109, C08S08, doi:10.1029/2003JC001800, 2004.

Webb, E. K., Pearman, G. I., and Leuning, R.: Correction of flux measurements for density effects due to heat and water vapour transfer, Q. J. Roy. Meteor. Soc., 106, 85–100, 1980.

Yelland, M., Pascal, R., Taylor, P., and Moat, B. I.: AutoFlux: an autonomous system for the direct measurement of the air–sea fluxes of CO_2, heat and momentum, Journal of Operational Oceanography, 2, 15–23, 2009.

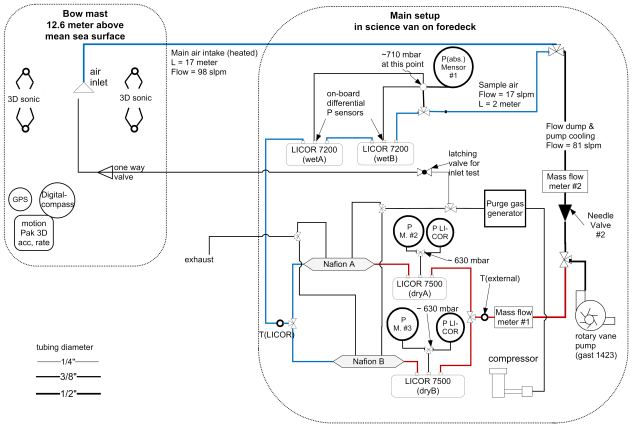

Fig. 1. Schematic of the Eddy Covariance setup for the SOAP experiment on the R/V *Tangoroa*. The sample air line is colour-coded in blue and the colour is changed to red downstream of the membrane dryers to indicate that the air is dried at this point.

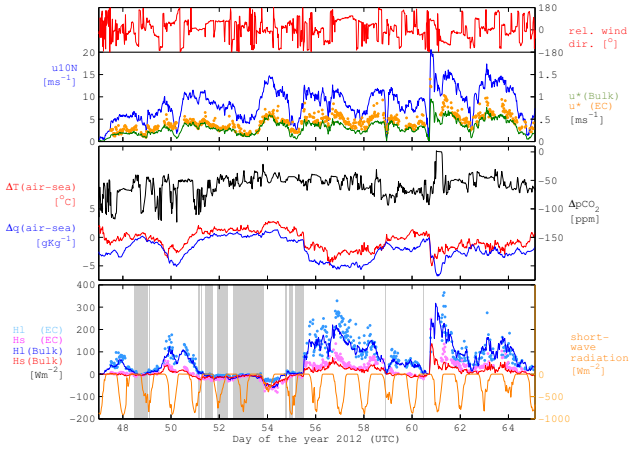

Fig. 2. Overview of conditions encountered during the SOAP experiment. Shaded areas mark low latent heat fluxes (Hl $\leq 7\,\mathrm{W\,m^{-2}}$). The wind speed measurement was taken on the ship's main deck and is corrected for air-flow-distortion (Popinet et al., 2004) and normalised to standard conditions (10 m height and neutral stability). This wind speed was used to calculated the bulk fluxes with the TOGA COARE 3.0 algorithm. All direct EC fluxes are measured at the bow mast using the Csat3 sonic anemometer and the IRGA in the science container on the fore-deck.

Table 1. Publications that are relevant for the bias in NDIR CO_2 measurements that is related to relative humidity.

Publication	Configuration	Notes
Kohsiek (2000)	two custom-made NDIR sensors	Laboratory test show dependency of the CO_2 on RH for RH $\geq 50\%$. Suggest water-films on the sensor optics as cause
McGillis et al. (2001)	LI-6262 closed-path with in-line particle filter	first air–sea EC CO_2 fluxes consistent with bulk formulas
Kondo and Osamu (2007)	LI-7500 open-path	measured CO_2 fluxes order of magnitude higher than bulk formula
Miller et al. (2010)	LI-7500 converted to closed-path, dried air-stream	reduced Webb correction CO_2 fluxes consistent with bulk formula
Prytherch et al. (2010a)	LI-7500 open-path + PKT	suggest water films caused by salt particles as cause; order of magnitude correction
Prytherch et al. (2010b)	LI-7500 open-path + PKT	transfer velocity measurements at high wind speeds; order of magnitude correction
Lauvset et al. (2011)	LI-7500 open-path + PKT	order of magnitude correction
Edson et al. (2011)	LI-7500 shrouded + PKT and spectral method	small particles on sensor lenses; order of magnitude correction
Kondo and Tsukamoto (2012)	LI-7500 open-path and LI-7000 closed path	measured CO_2 fluxes from both sensors order of magnitude higher than bulk formula
Huang et al. (2012)	LI-7500 open-path on buoy	PKT results not plausible
Ikawa et al. (2013)	LI-7500 open-path on coastal tower	PKT results not plausible
This study	LI-7500 Miller et al. (2010) compared to LI-7200 closed path + PKT	dry CO_2 fluxes consistent with bulk formula; un-dried CO_2 fluxes biased low; disproves PKT correction

Table 2. Average CO_2 fluxes in $[\mathrm{mol\,m^{-2}\,yr^{-1}}]$ for the complete experiment, and for subsets (Subset 1 $[-7\,\mathrm{W\,m^{-2}} \leq \mathrm{Hl} \leq +7\,\mathrm{W\,m^{-2}}]$; Subset 2 $[-35\,\mathrm{W\,m^{-2}} \leq \mathrm{Hl} \leq -7\,\mathrm{W\,m^{-2}}]$; Subset 3 $[+7\,\mathrm{W\,m^{-2}} \leq \mathrm{Hl} \leq 340\,\mathrm{W\,m^{-2}}]$) based on the EC latent heat flux measured by the un-dried gas analysers. To make the values comparable, only intervals with results from the PKT loop are used for the calculating the mean flux values.

Interval	all	Subset 1	Subset 2	Subset 3
# intervals	161	28	24	109
F_{cm} *dryA*	−7.21	−6.59	−5.80	−7.69
F_{cm} *dryB*	−7.16	−6.51	−5.63	−7.66
F_{cm} *wetA*	+5.01	−6.50	−7.67	+10.76
F_{cm} *wetB*	−3.29	−5.96	−6.62	−1.87
F_{PKT} *wetA*	−2.34	−5.89	−8.97	+0.03
F_{PKT} *wetB*	−3.09	−6.67	−7.94	−1.10

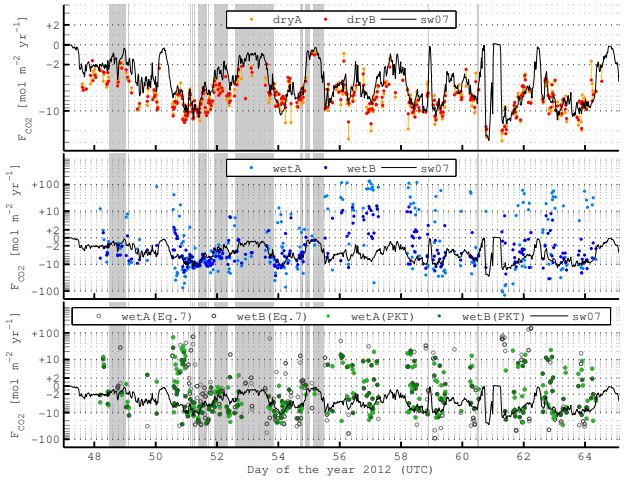

Fig. 3. Time series of the direct CO_2 fluxes and the flux calculated with the parameterisation of Sweeney et al. (2007), plotted on logarithmic scale with sign. Values between $\pm 2\,\mathrm{mol\,m^{-2}\,yr^{-1}}$ are plotted on linear scale. Shaded areas mark low latent heat fluxes ($\mathrm{Hl} \leq 7\,\mathrm{W\,m^{-2}}$). Top: fluxes from *dryA* and *dryB* parallel measurements are linked with vertical lines; middle: fluxes from *wetA* and *wetB*; bottom: fluxes from *wetA* and *wetB* after the PKT correction has been applied to the CO_2 measurements and the results from Eq. (7), which are overlaid with the PKT results.

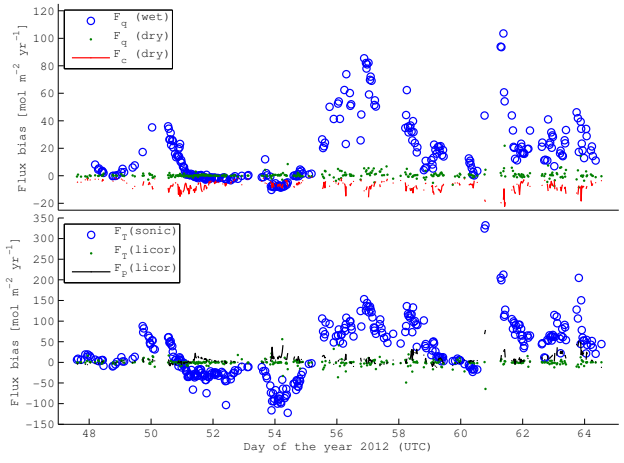

Fig. 4. Time series of the bias fluxes in Eq. 3, caused by air density fluctuations (Webb et al., 1980). Top: Bias flux caused by humidity fluctuations F_q upstream of the dryer *wet* and downstream *dry* and the CO_2 flux F_c as measured by the IRGA *dry* (there are only small differences between *A* and *B*). Bottom: Bias flux caused by temperature fluctuations F_T as measured by the bow mast sonic and as measured by the CP-IRGAs, and the bias flux caused by pressure fluctuations F_P.

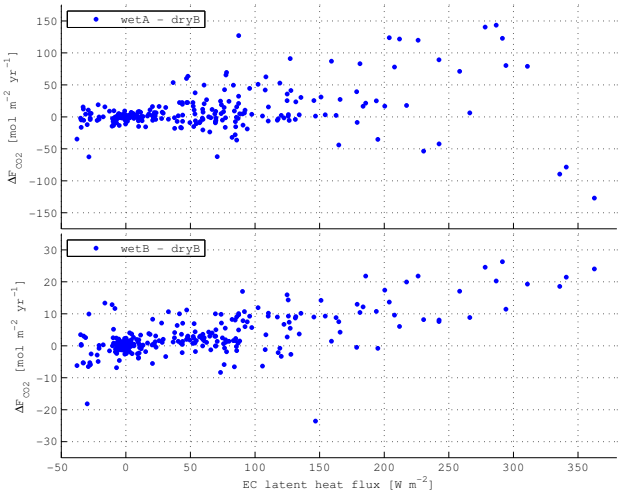

Fig. 5. Difference between the CO_2 flux calculated from the measured signals x_{cm} from the un-dried gas analysers to the flux from *dryB* as a function of the EC latent heat flux measurement from the un-dried gas analysers. Different scales are used for the two subplots.

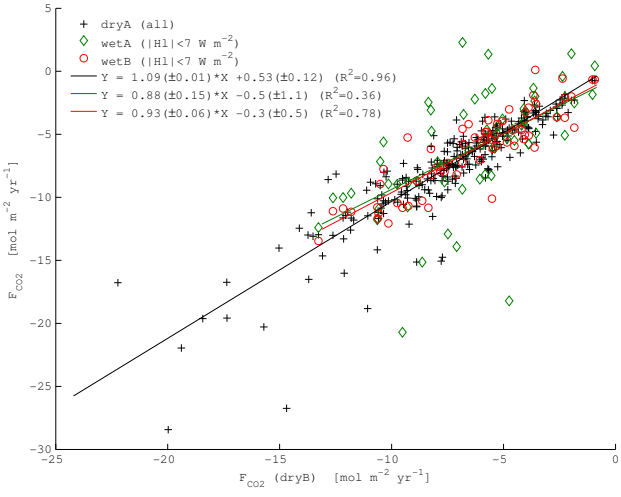

Fig. 6. Scatter plot of the CO_2 flux measurements (without PKT correction) from *wetA*, *wetB* and *dryA* against those from *dryB*. For *wetA* and *wetB*, only measurements with $\mathrm{Hl} \leq 7\,\mathrm{W\,m^{-2}}$ are used. Linear fit coefficients with standard deviation and the R^2 value are shown in the legend.

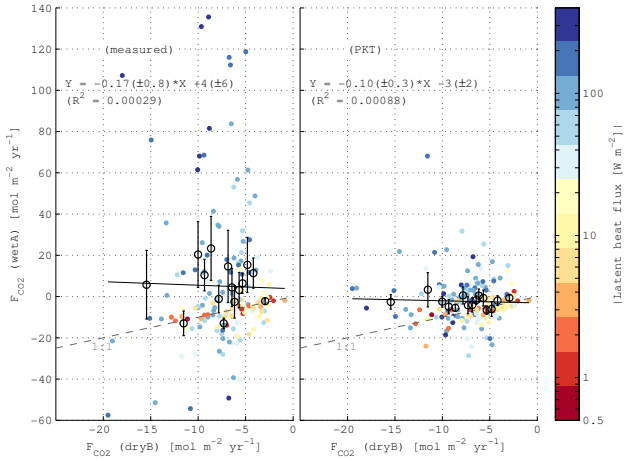

Fig. 7. Scatter plot of the CO_2 flux measurements from *wetA* against those from *dryB* before (left) and after the PKT correction was applied to the *wetA* measurements (right). Bin averages of 15 bins with an equal number of data points are shown as black circles, with error bars indicating the standard deviation from the bin average. A linear regression to the data is shown as solid black line and the $1:1$ agreement is indicated with a grey dashed line. Only intervals for which the PKT correction provided a result for both, *wetA* and *wetB*, were used for this plot.

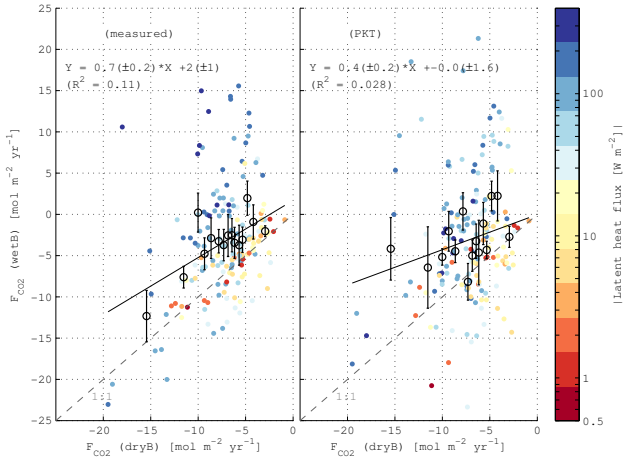

Fig. 8. Same as Fig. 7, but for *wetB*.

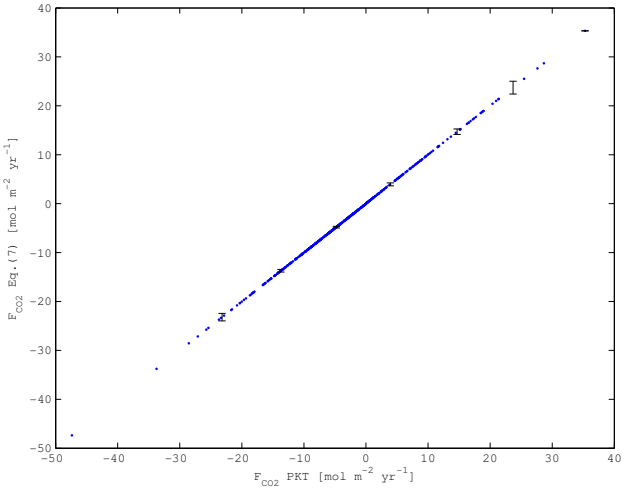

Fig. 9. Scatter plot of the results from Eq. (7) against the results of the PKT correction for IRGA wetB, individual (blue) and binned (black).

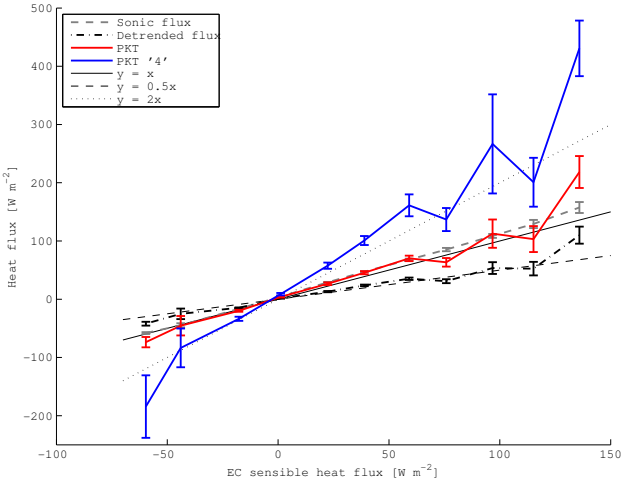

Fig. 10. Bin-averaged heat fluxes plotted against the standard EC sensible heat flux results (to be compared with Fig. 2 in Prytherch et al., 2010a): "sonic flux" calculated from T_s (light grey - -); flux after detrending against humidity (black -.); "PKT-corrected" flux (red -); results of a PKT correction with step width 0.75 and $\beta \approx 4$ ("PKT 4") (blue -). Error bars show standard deviation from the mean. $1:1$, $1:2$ and $2:1$ agreement are indicated.

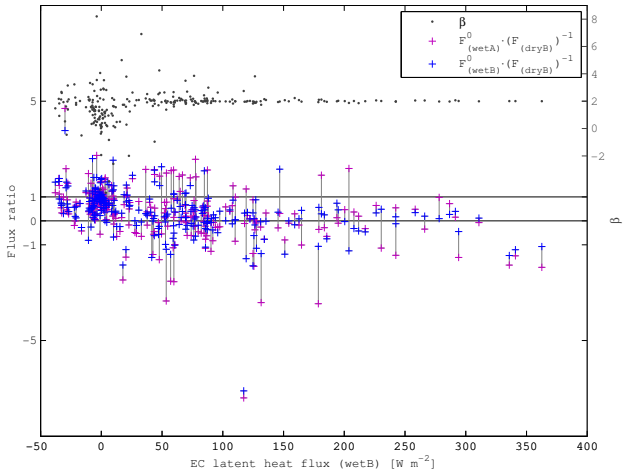

Fig. 11. Ratio of the detrended CO_2 fluxes F_c^0 from *wetA* and *wetB* as used for the PKT correction to the CO_2 flux calculated from *dryB* (purple $+$, blue $+$). Two values of the same sample interval are connected with a grey line; the factor $\beta = \left(1 - 0.5 \frac{\langle \mathrm{RH}' w' \rangle}{\langle x_\mathrm{v}' w' \rangle} \frac{\partial \langle x_\mathrm{v} \rangle}{\partial \langle \mathrm{RH} \rangle}\right)^{-1}$ as in Eq. (7), calculated from the latent heat flux and relative humidity, as measured by *wetB*, (grey $\bullet$). The PKT-corrected fluxes are the product of F_c^0 and β. The black lines indicate the ratios zero and one.